

REPORT DOCUMENTATION PAGE

0585

1. AGENCY USE ONLY (Leave blank)		2. REPORT DATE 10-23-97	3. REPORT TYPE AND DATES COVERED Final Technical Report
4. TITLE AND SUBTITLE Anode Current Attachment in Collisional Plasmas			5. FUNDING NUMBERS F49620-95-C-0031
6. AUTHOR(S) G. W. Butler			
7. PERFORMING ORGANIZATION NAME(S) AND ADDRESS(ES) Boeing Information, Space & Defense Systems Research and Technology 20403 68th Ave. So. Kent, WA 98032			6. PERFORMING ORGANIZATION REPORT NUMBER
9. SPONSORING / MONITORING AGENCY NAME(S) AND ADDRESS(ES) AFOSR/NA 110 Duncan Avenue, Suite B115 Bolling AFB, DC 20332-001			10. SPONSORING MONITORING AGENCY REPORT NUMBER
11. SUPPLEMENTARY NOTES			
12a. DISTRIBUTION / AVAILABILITY STATEMENT Approved for public release, distribution unlimited			12b. DISTRIBUTION CODE
13. ABSTRACT (Maximum 200 words) Improvements in arcjet performance are primarily limited by the anode's ability to process the energy densities associated with arc attachment. The motivation for this work was our lack of understanding of these processes. The more global objective was to develop an understanding of arc attachment physics and energy transfer to anode surfaces in collisional plasmas. A numerical multifluid approach was formulated to investigate the behavior of the plasma at an anode surface, taking into account the motion and interaction of electron, ion, and neutral fields with the solid conducting boundary. Attempts to validate the numerical algorithm have not yet proven successful. Two different approaches have been explored, but both have demonstrated numerically divergent solutions. Without the clear demonstration of success, efforts to compare with experimental data have been postponed. Continued work with this numerical approach will generate a physical correct and correlated approach to estimating the thermal loading due to the attachment of high intensity, high velocity arcs at near-atmospheric pressures. The results of this effort could not only be used to design arcjet electrodes, but also other high current devices, such as plasma switches and relays.			
14. SUBJECT TERMS Anode, collisional plasmas, multifluid analysis, current attachment			15. NUMBER OF PAGES 9
			16. PRICE CODE
17. SECURITY CLASSIFICATION OF REPORT Unclassified	18. SECURITY CLASSIFICATION OF THIS PAGE Unclassified	19. SECURITY CLASSIFICATION OF ABSTRACT Unclassified	20. LIMITATION OF ABSTRACT UL

ANODE CURRENT ATTACHMENT IN COLLISIONAL PLASMAS

AFOSR Contract Number F49620-95-C-0031

G.W. Butler

The Boeing Commercial Space Company
P.O. Box 3999, MS 6E-01
Seattle, Washington 98124-2499

Summary

Improvements in arcjet performance are primarily limited by the anode's inability to process the energy densities associated with arc attachment. The motivation for this work was our lack of understanding of these processes. The more global objective was to develop an understanding of arc attachment physics and energy transfer to anode surfaces in collisional plasmas. Three program phases were planned: Phase 1 required the development of a self-consistent numerical algorithm for collision-dominated plasmas; Phase 2 sought to compare this approach to published numerical solutions for weakly ionized plasmas; and Phase 3 was to compare predictions of high current density, strongly ionized plasmas with experiments carried out under other AFOSR funding. With reasonable success in this final phase, the multifluid model was to be to provide guidance for the design of next generation arcjet technology.

The numerical multifluid approach formulated in Phase 1 described the behavior of the plasma at an anode surface, taking into account the motion and interaction of electron, ion, and neutral fields with the solid conducting boundary. Phase 2 attempts to validate the numerical algorithm have not yet proven successful. Two different approaches have been explored, but both have demonstrated numerically divergent solutions. Without clear success in the Phase 2 effort, the comparison with experimental data in the Phase 3 was postponed.

Continued work with this numerical approach will generate a physical correct and correlated approach to estimating the thermal loading due to the attachment of high intensity, high velocity arcs at near-atmospheric pressures. The results of this effort could not only be used to design arcjet electrodes, but also other high current devices, such as plasma switches and relays.

DTIC QUALITY INSPECTED 3

19971118 038

Background

Low power arcjet thrusters (≤ 2 kW) are high specific impulse, high specific energy electric propulsion devices that are now used for north-south satellite stationkeeping. Arcjet performance can be used to meet future mission scenarios if their performance can be improved to accomplish other necessary functions such as orbit transfer or repositioning. To maintain a competitive advantage, these additional on-orbit requirements can only be accomplished by operating at significantly higher specific energies without a loss in thrust efficiency. Unfortunately, present data would indicate that anode materials are now approaching their design limits.

The management of the anode thermal loading¹ is thus the most critical area for performance improvement. An understanding of the physical processes that govern arc attachment and heat transfer to the anode is essential (particularly in the vicinity of the arcjet throat). Although numerical models are capable of providing data for critical design decisions, their accuracy depends on correctly modeling the underlying physics of arc attachment and heat transfer at the anode-plasma boundary -- a task most often estimated in single-fluid approaches by electrode-wall models. The multifluid approach has potential to improve upon single-fluid techniques by providing separate descriptions for the electron, ion, and neutral fields and their exchange of mass, momentum, and energy.

Objective

The objective of this work was to develop and verify analytical models which yield insights to the key physical processes governing arc attachment and the thermal loading of anodes in collisional plasmas.

Technical Approach

The technical challenge of this effort was to extend the multifluid analysis for weakly ionized plasmas of Meeks and Cappelli² to significantly higher current densities and highly compressible plasmas typical of arcjet thrusters.

The effort divided naturally into three phases:

Phase 1: The construction of a multifluid model of the arc attachment process.

Phase 2: Validation of the Phase 1 model by direct comparison with the recent work of Meeks and Cappelli.² Rationalize differences and refine the model where necessary.

Phase 3: Investigation of arc attachment phenomena at higher current densities where significant coupling exists between the arc and bulk plasma. This included a comparison of model predictions with experimental data from other AFOSR research programs.

Our approach was to solve the weakly ionized stagnation point flow problem posed by the authors of Reference 2 and to directly compare the results of the two analyses. The baseline test case shown in Figure 1 is similar to that of used in Meeks and Cappelli.² The bulk flow is always toward the anode. The plasma constituents are Ar (Class 1), Ar^+ (Class 2), and electrons, E (Class 3). The anode surface temperature T_w is assumed constant.

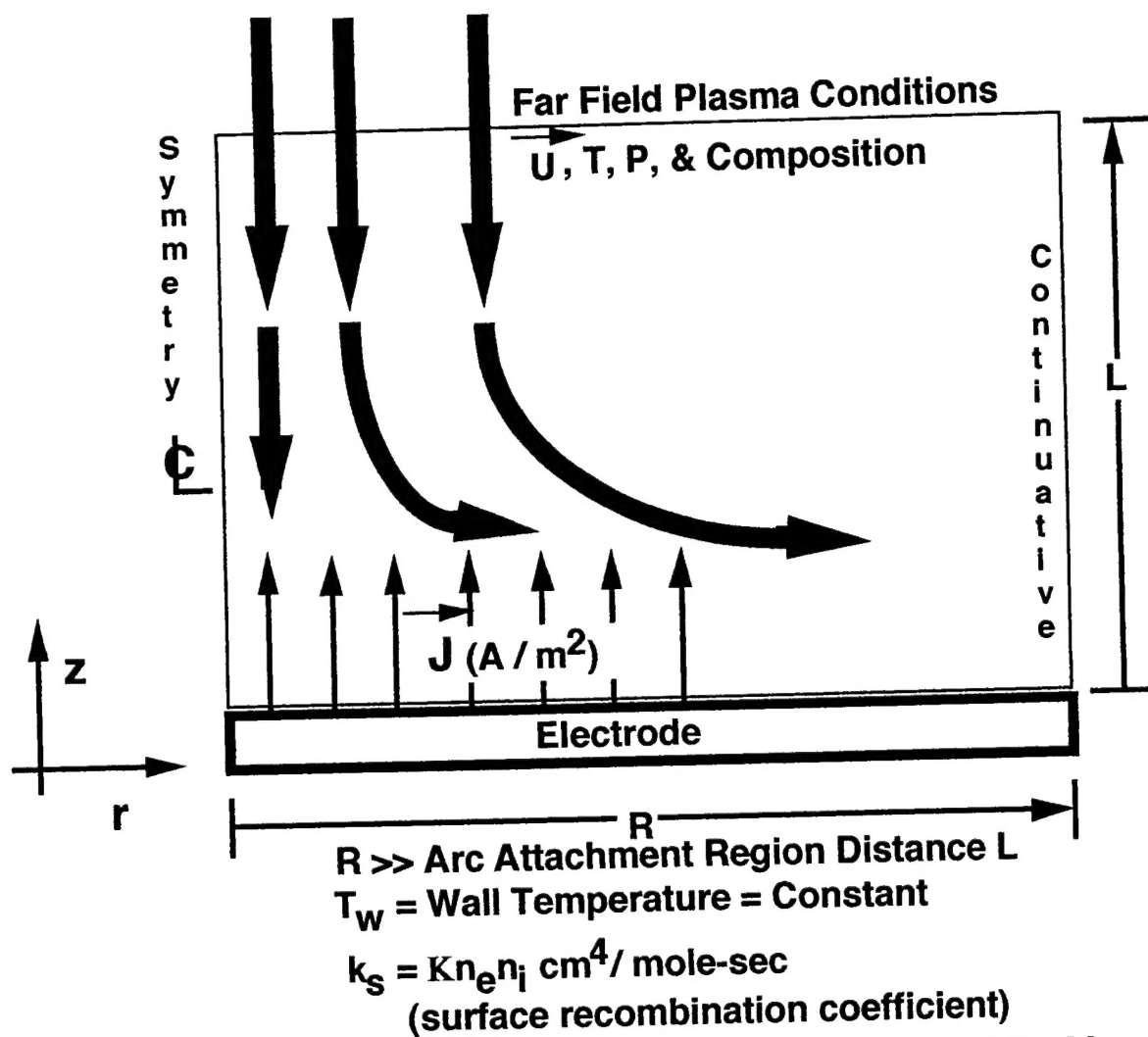


Figure 1. Schematic of the Point-Plane Arc Attachment Problem

The specification of the incident current density along this surface also determines the boundary condition for the magnetic field strength at the surface. In this case, the neutral and ion class velocities were assumed to obey the no-slip condition. The electrons, however, carry the full current and pass unhindered with a trajectory normal to the surface. The radial dimension of the attachment zone, the magnitude of the flux density, and a surface recombination rate must also be specified. The free stream conditions are taken to represent the far-field plasma state. The individual class temperature, pressure, velocity, and chemical composition must be specified. Unlike the approach in Reference 2, the ion and electron velocities as well as the magnetic field are free to change along this surface as the solution for current density evolves.

The center of the arc column is a line of symmetry for all plasma parameters with the radial extent of the computational space a distance R from the centerline. The assumption is that if R is chosen large enough, the influence of the boundary diminishes and the solution near the arc-centerline better represents the one-dimensional similarity solutions of Reference 2. The choices for other parameters along the R -surface, however, are less obvious. The approach taken here was to set the magnetic field to zero along this boundary to limit the current to the computational space. The ion and electron class boundary conditions along the surface were treated as continuative (i.e., the values of the variables do not change across the boundary). Finally, the neutral class pressure (P) or pressure gradient parameter (defined as $\Lambda = \frac{1}{r} \frac{\partial P}{\partial r}$ in Reference 2) was set to a constant value.

Results: Phase 1

A multifluid description of the attachment process has been developed to represent the behavior of neutrals, ions, and electrons within a plasma. There are no restrictions relative to the populations of each field. Each particle class has its own velocity and temperature distribution (energy) and is coupled to the other classes by inter-class mass, momentum, and energy exchange processes. The derivation of these multifluid conservation equations, auxiliary state relationships, and exchange terms have been discussed in previous work.^{3,4} Note that in the model equations shown in Figure 2, the magnetic field (\vec{B}) is a primary variable and the electric field (\vec{E}) and associated potential (Φ) are derived quantities.

The Phase 1 work produced two numerical approaches to the solution of these equations and the construction of the associated algorithms (i.e., Algorithm 1 and Algorithm 2). The two approaches differed fundamentally in the construction of the solver for Φ .

Algorithm 1 Φ -Solver

Construction of the Algorithm 1 Φ -solver was completed early in the program and initially validated by comparison of its solution with a number of readily available static test cases.

Incorporation of the Φ -solver with the parent multifluid code was straightforward since it was constructed to operate on the same mesh as that used for the plasma.

The logical flow of the solution in the Algorithm 1 is briefly described here. It consists of a Lagrangian phase in which the state of individual mass elements in each field are advanced in time and position, followed by a remap of those states onto the Eulerian grid. The ion and neutral field momentum equations are first solved for the respective Lagrangian velocities \bar{u}_n and \bar{u}_i , assuming all other state parameters are known. The subscripts n and i refer to the neutral and ion fields. Solving Equation 6 for \bar{B} with the electron velocity, \bar{u}_e , assumed known leads to a solution for the total current density \bar{J} (Equation 5). Subtracting the ion current from \bar{J} leads directly to the electron current and an updated value for \bar{u}_e . With the updated estimates for velocities, and additional sources of energy transport calculated (e.g., chemical energy release, Ohmic heating, etc.), the energy transport (Equation 3) is solved for the different field energies. At this point, the exchange of mass, momentum, and energy between the different classes is accomplished using appropriate collision cross sections and exchange coefficients.⁴ Finally, all the Lagrangian state variables are mapped from the Lagrangian space back onto the Eulerian grid. This cycle is repeated until a steady state solution is obtained.

Static plasma calculations (i.e., all initial field velocities set to zero) demonstrated the anticipated null-solutions without spurious numerical errors. Differences from cycle-to-cycle were on the order of the anticipated numerical round off. However, for plasmas with non-zero velocities, the numerical solution slowly diverged, demonstrating a continually increasing spatial charge density, or non-neutral plasma condition. This scenario, of course, violates the charge-neutrality assumption upon which the algorithm is based and led to re-evaluation and eventual redesign of the numerical approach. The refined methodology, Algorithm 2, is discussed in the following section.

Algorithm 2 Φ -Solver

An evaluation of the Algorithm 1 solution suggested the need for a self-consistent, conservative solution method. The principle problem exposed by the approach taken in Algorithm 1 was that the prediction for the electron velocity depended on the ion velocity estimate which, in turn, was derived from the total current density. Note that the current density depends on \bar{B} and the initial estimate for \bar{u}_e . An error in any of one of these steps leads to further propagation of errors and decreasing solution fidelity.

An alternate solution (Algorithm 2) method suggested by Brackbill⁵ makes use of the equivalent quasi-neutrality condition $\nabla \cdot \bar{J} = 0$ where \bar{J} is the total current, to provide an indirect calculation of the electron current. Following Brackbill, the inertial terms in the electron momentum equation (Equation 2) are neglected ($\rho_e d\bar{u}_e/dt \approx 0$) and an equation for the electron

CONSERVATION OF MASS:

$$\frac{d_s(\rho_s V_s)}{dt} = \dot{\rho}_s V_s, \text{ where } \frac{d_s V_s}{dt} = V_s (\nabla \cdot \vec{u}_s) \text{ and } \dot{\rho}_s = \sum_{s(r)} P_r^\# - P_r^* \quad (1)$$

CONSERVATION OF MOMENTUM:

$$\frac{d_s(\rho_s \vec{u}_s V_s)}{dt} = V_s \left[-\nabla p_s + \nabla \cdot \tilde{\tau}_s + \tilde{\vec{E}}_s \sum_{s(r)} Z_r n_r q + \sum_{s(r)} (P_r^\# \vec{u}_s - P_r^* \vec{u}_s) + \sum_{t(l)} K_{lk} (\vec{u}_t - \vec{u}_s) \right] \text{ where } \tilde{\vec{E}}_s = \vec{E} + \frac{1}{c} \vec{u}_s \times \vec{B} \quad (2)$$

CONSERVATION OF ENERGY:

$$\frac{d_s(\rho_s e_s V_s)}{dt} = V_s \left[-P_s \nabla \cdot \vec{u}_s + \nabla \cdot (K_s \nabla T_s) + \Phi_s + \sum_{s(r)} (P_r^\# e_r - P_r^* e_r) + \sum_{t(l)} R_{kt} (T_t - T_s) + \sum_{t(l)} S_{kl} (\vec{u}_t - \vec{u}_s)^2 \right] \quad (3)$$

FARADAY'S LAW:

$$\nabla \times \vec{E} = -\frac{1}{c} \frac{\partial \vec{B}}{\partial t} \quad (4)$$

AMPERE'S LAW:

$$\vec{J} = \frac{c}{4\pi} (\nabla \times \vec{B}) \quad (5)$$

(Neglecting Displacement Current)

$$\frac{\partial \vec{B}}{\partial t} = \nabla \times \vec{u}_e \times \vec{B} - \nabla \times \eta (\nabla \times \vec{B}) + \nabla \times \frac{c}{n_e q} [\nabla P_e - K_{en} (\vec{u}_n - \vec{u}_i)] \quad (6)$$

INDUCTION EQUATION:

$$\text{EQUATION OF STATE (PERFECT GAS):} \quad P_s = \sum_{s(r)} n_r k T_s \quad (7)$$

ELECTRIC POTENTIAL:

$$\nabla^2 \cdot \Phi = -4\pi q \quad (8)$$

Figure 2.0 Multifluid Equations for the Plasma

current density is then derived by multiplying Equation 2 by q/m_e where q_e is the electron charge and m_e is the electron mass:

$$\vec{J}_e - \frac{\vec{J}_e \times \vec{\Omega}_e}{\eta_e} = \frac{\omega_{pe}^2}{\eta_e} \vec{E} + \vec{S}_e$$

where $\omega_{pe}^2 = \frac{n_e q_e^2}{m_e}$ is the electron plasma frequency squared, $\vec{\Omega}_e = \frac{q_e |\vec{B}|}{c \cdot m_e}$ is the electron

cyclotron frequency, $\eta_e = \sum_i \frac{q_i K_{ie}}{m_e \cdot n_e}$ the resistivity, and

$$\vec{S}_e = \frac{1}{\eta_e} \left[\frac{q_e}{m_e} (-\nabla P_e + \nabla \cdot \tau_e) + \dot{\vec{J}}_e - \sum_{i \neq e} K_{ie} \vec{J}_i \right].$$

Following Brackbill's derivation and writing expressions for $\vec{J}_e \times \vec{\Omega}_e$ and $\vec{J}_e \cdot \vec{\Omega}_e$ to solve for \vec{J}_e , leads to an expression for the electron current density:

$$\vec{J}_e = \frac{1}{(1 + \vec{\Omega}_e'^2)} \cdot \left\{ \omega_{pe}'^2 \left[\vec{E} + \vec{E} \times \vec{\Omega}_e' + (\vec{E} \cdot \vec{\Omega}_e') \vec{\Omega}_e' \right] + \left[\vec{S}_e + \vec{S}_e \times \vec{\Omega}_e' + (\vec{S}_e \cdot \vec{\Omega}_e') \vec{\Omega}_e' \right] \right\}$$

where $\omega_{pe}' = \frac{\omega_{pe}}{\eta_e}$ and $\vec{\Omega}_e' = \frac{\vec{\Omega}_e}{\eta_e}$. Using $\nabla \cdot \vec{J} = 0 = \nabla \cdot (\vec{J}_e + \vec{J}_i)$ and assuming that \vec{J}_i is known from the previous ion momentum equation, an equation for \vec{E} can be derived:

$$\nabla \cdot (\epsilon \cdot \vec{E}) = -\nabla \cdot \vec{S}_e - \sum_{i \neq e} \vec{J}_i.$$

This equation can be solved for Φ assuming that $-\frac{1}{c} \frac{\partial \vec{B}}{\partial t} = \nabla \times \vec{E} \approx 0$ which in turn leads to the approximation $\vec{E} = -\nabla \Phi$.

The logical flow of Algorithm 2 then follows:

1. Solve for the rate of change of plasma species, $\dot{\rho}_s$,
2. Solve the momentum equation for both ions and neutrals
3. Evaluate the ion current, \vec{J}_i
4. Solve for the potential field and the electric field
5. Solve for the electron velocity
6. Solve for the magnetic field using Ampere's Law
7. Advance the neutral, ion, and electron energy equations

8. Return to the top of the cycle and begin again.

Although this scheme proved more difficult to implement than that of Algorithm 1, the solutions obtained for flowing plasmas with simple boundary conditions were stable and remained quasi-neutral regardless of calculation time.

Comparison of the Algorithm 2 results with the weakly ionized solutions of Reference 2, however, again proved unsuccessful, largely due to difficulties in implementing the more complex boundary conditions. Small errors introduced by the numerical approach at the boundaries propagated into the computational space, eventually corrupting the solution. A complete investigation of this problem and possible solutions were not completed before the end of the present contract period.

Conclusions

This work has exposed shortcomings with standard multifluid approaches. It has also investigated an promising approach using a method outlined by Brackbill⁵ to solve the multifluid equations. Further work is required to understand and implement boundary conditions in this new scheme. The completion of this task, however, is essential if we are to compare the more general multifluid approach with the work of Reference 2 or to gain further insight into the physics of arc attachment.

References

1. Butler, G.W. and Cassady, R.J., "Directions for Arcjet Technology Development," *Journal of Propulsion and Power*, Vol. 12, Number 6, November-December, 1996.
2. Meeks, E. and Cappelli, M.A., "Multifluid Stagnation Flow Plasma Model with Self-Consistent Treatment of the Collisional Sheath," *IEEE Transactions on Plasma Science*, Vol 21, Dec. 1993.
3. Butler, G.W. and King, D.Q., "Single and Two Fluid Simulations of Arcjet Performance," Presented at the AIAA/SAE/ASME/ASEE 28th Joint Propulsion Conference and Exhibit, Nashville, TN, July 6-8, 1992.
4. Burgers, J.M., Flow Equations for Composite Gases, Vol. 11 of Applied Mathematics and Mechanics, edited by Frenkiel, F.N. and Temple, G., Academic Press, New York, 1969.
5. Personal Communication. "An Implicit-Time Discretization of the Equations for a Collisional, Multi-Fluid Plasma," Los Alamos National Laboratory Memorandum to Bryan Kashiwa, T-3, B216, February 14, 1994 from J. Brackbill, T-3, B216.

Directions for Arcjet Technology Development

G. W. Butler* and R. J. Cassady†
Olin Aerospace Company, Redmond, Washington 98052

Guidelines for improvements in arcjet performance based on a simplified analysis of advanced mission requirements are presented. The results of this analysis clearly show that to remain competitive with next-generation electric propulsion devices, significant increases in the specific impulse of present arcjet technology must be achieved. Of the various design options available, concepts that improve the thrust efficiency offer the greatest performance leverage, and may, in fact, represent the only approaches capable of meeting the advanced mission goals. If they are to be successful, such concepts will improve the management of energy and mass transport within the arcjet. One method to understand and control the internal plasmadynamics of the arcjet to improve its performance is outlined.

Nomenclature

H^*	= excited state hydrogen atom
I_{sp}	= specific impulse, s
\dot{m}	= propellant mass flow rate, mg/s
N_2H_4	= monopropellant hydrazine
P	= power delivered to the propulsion system, W
P_c	= chamber pressure, MPa
P_n	= power delivered to the propellant (plasma), W
P_n/\dot{m}	= specific energy, J/kg
T/P	= thrust-to-power ratio, N/W
W-100	= pure tungsten metal
W-2%ThO ₂	= thoriated tungsten
W-4%Re-0.3%HfC	= tungsten-rhenium-hafnium carbide alloy
ΔV	= velocity increment, m/s
η	= thrust efficiency, %
η_{pcu}	= power conditioning unit conversion efficiency, %
σ_e	= electrical conductivity

Introduction

ARCJET thrusters are high specific impulse, high specific energy, electric propulsion (EP) devices now in use for North-South (N-S) satellite stationkeeping of geosynchronous satellites. At present, low-power arcjets operate on hydrazine decomposition products and afford an I_{sp} in the 500–600-s range with η of approximately 30–35%. Figure 1 presents a schematic of the physics at work within a conventional arcjet thruster. The discharge is a wall- and vortex-stabilized arc. The arc emanates from the cathode, passes through the constrictor, and attaches in a diffuse (nondestructive) manner along the expanding portion of the nozzle (anode). The propellant is injected upstream of the cathode tip with an azimuthal component of velocity. The resultant swirl promotes arc stability and acts to reduce heat transfer to the upstream anode surfaces. The propellant merges with the arc as it passes from the plenum through the constrictor, into the expanding portion of the nozzle, and finally to ambient space. The merging of the arc with the propellant gas is a complex and continuous process. No distinct boundary between arc and nonarc fluid can be drawn.

The shaded zones of Fig. 1 identify regions of the discharge in which different physical processes may be considered dominant. The principal activity in zone 1 is the dissipation of electrical energy via collisions of electrons with the neutral and ionized propellant. Some of the ions produced in this region migrate to the cathode with sufficient energy to maintain the discharge. The bulk of the current is made up of electrons that travel through the propellant under the influence of the electric field to the anode. They are continually decelerated by collision with their heavier neighbors and continually accelerated by the imposed electric field. In zone 2, this process results in a substantial increase in the bulk temperature of the plasma. This situation changes dramatically as the plasma leaves the constrictor and enters zone 3, which is characterized by decreasing field strengths and rapid gasdynamic expansion of the plasma. Thermal energy exchange between the electrons and other species thus falls dramatically so that this region is dominated by the evolution of energy from recombination reactions. In zone 4, the conversion of this internal energy to kinetic energy occurs through gasdynamic expansion processes. In this zone, viscous dissipation and heat transfer at the anode surface reduce the benefits of the expansion process.

Typical low-power arcjets have conical converging-diverging nozzles with constrictor diameters on the order of 0.05 cm, nominal expansion angles of 20 deg, and exit diameters of 0.35 cm. Moving up in power to 30 kW, representative constrictor and exit dimensions increase to 0.5 and 2.5 cm, respectively.

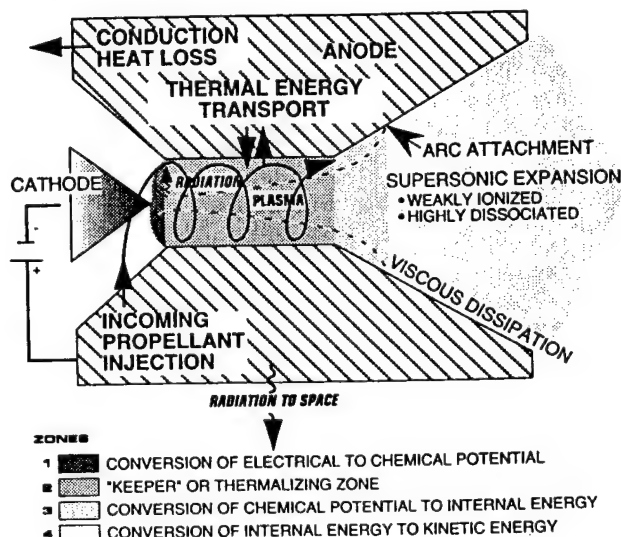


Fig. 1 Key features of the arcjet physics.

Received Nov. 2, 1994; revision received Feb. 15, 1996; accepted for publication Aug. 17, 1996. Copyright © 1996 by the American Institute of Aeronautics and Astronautics, Inc. All rights reserved.

*Senior Staff Engineer, P.O. Box 97009.

†Project Team Leader, P.O. Box 97009.

The physical characteristics of the arcjet flowfield vary from a nearly fully ionized plasma at temperatures in excess of 20,000 K near the cathode tip to a relatively cold plasma (1000–2000 K) at the anode surface. Moreover, velocities vary from approximately 10 km/s on centerline to zero at the wall. Considering the magnitude of these parameters and small geometric length scales, it is clear that the arcjet's performance depends largely on nonequilibrium transport processes.

Future mission scenarios discussed in the following section reflect the need for greater control of on-orbit assets. The stationkeeping roles of present low power arcjets must expand to include orbit maneuvering and some limited number of repositioning events. For the arcjet, this will require even higher I_{sp} , which, in turn, means driving their operational envelope to higher specific energies (P_n/\dot{m}) while maintaining or improving thrust efficiency.

The present-day technology, however, is limited by the anode's ability to withstand the high thermal fluxes that are characteristic of operation at high P_n/\dot{m} (e.g., higher power dissipation and/or lower mass flow rates). In fact, many prototype thrusters fail in extended life tests because of the intolerable heat loads on the anode. A significant performance improvement without loss of useful life must therefore be achieved through some combination of higher P_n/\dot{m} , higher I_{sp} , or higher η . The motion of the plasma, the large gradients in chemical composition and fluid properties, and the relatively short residence times make this a formidable design problem.

Advanced Mission Requirements

The mission applications for on-orbit propulsion can be generally collected into three categories: 1) stationkeeping, 2) maneuvering, and 3) transfer. These functions were referred to in a recent study even more simply as 1) hold, 2) move, and 3) lift.¹ We will describe each of these functions and the implications of improvements in arcjet performance. Arcjet performance for both a baseline and an advanced technology level will be compared with other EP thruster systems. Table 1 lists the parameters assumed for each propulsion system separated into categories of hold and move and lift.^{2–5} The system power is defined as the power to the power conditioning unit (PCU) and the life and total impulse numbers are the assumed capabilities of a single thruster.

Hold

Hold maneuvers maintain a spacecraft in a given orbit. Examples include (N–S) and East–West (E–W) stationkeeping of geosynchronous (GEO) communications satellites and drag makeup for low earth orbit (LEO) satellites. Thrust levels are not a primary consideration because the perturbing force is of low magnitude. Higher I_{sp} is the more important performance parameter since the fuel mass required for the mission must be minimized. Electric propulsion is well suited to this require-

ment. In fact, electric propulsion devices such as pulsed plasma thrusters (PPTs) and electrothermal hydrazine thrusters (EHTs) have been routinely used since the early 1980s for drag makeup and N–S stationkeeping,^{6,7} respectively. In early 1994, arcjets were used for the first time aboard the Telstar 401 satellite for N–S stationkeeping.

The EP systems described in Table 1 were evaluated for the N–S stationkeeping mission of a GEO satellite with an initial mass of 1500 kg. Satellite lifetime was varied from 10 to 15 years. Power delivered to the propulsion systems was assumed to be limited to 4 kW. Thruster concepts were assumed to use the demonstrated power level for the particular device listed in Table 1 and the number of thrusters was scaled to come as close as possible to 4 kW. Using parametric analysis, the total propulsion system mass was evaluated as a function of payload. The EHT (300-s MR-502) system mass is highest across the range of ΔV required for a 10–15-year mission. The baseline arcjet (502-s MR-508) falls in an intermediate range. An improved arcjet (650 s) is much more competitive on a system wet mass basis with the 30-cm ion engine and the SPT-100 Hall thruster.

The second consideration in the application trades is the time required to perform the stationkeeping maneuver. This is inversely proportional to the thrust level of the EP device. For a fixed power level delivered to the propulsion system, this trade favors a device with a high T/P , as shown in Fig. 2. It is also important to maintain or improve thrust efficiency as shown by

$$\eta = \frac{\dot{m}U^2}{2P_n} = \frac{T^2}{2\dot{m}P_n} = \frac{gI_{sp}}{2} \left(\frac{T}{P_n} \right) = \frac{gI_{sp}}{2\eta_{pcu}} \left(\frac{T}{P} \right) \quad (1)$$

Reduced thrust efficiency requires longer or more frequent thruster burns to perform the hold mission, complicating battery and power distribution system designs. In general, longer burns are less desirable to users because mission operations (ground control) become more complex. Another consideration is the life testing that drives the cost to qualify the system. Typical users require the demonstration of lifetime 1.5 times the mission life. Obviously, systems that require longer thruster life will cost more to qualify.

Figure 3 shows approximate operational envelopes for current and advanced arcjet technology. Increasing I_{sp} in the 1.5–2.0-kW power range is critical to hold mission applications. This will make arcjet systems mass competitive with the advanced Hall and ion thruster systems for payloads up to 1500 kg and mission lifetimes of up to 15 years. Because of the user concern over operational issues, it is also important to maintain η as I_{sp} is increased to minimize the frequency and duration of thruster firings.

Table 1 EP systems summary

Name	System power, W	Thrust, N	I_{sp} , s	Life, h	Inert mass, kg	Tank fraction	Total impulse capability, N-s
Hold and move propulsion systems							
MR-502 EHT	750	3.90E-01	302	370	1.85	0.04	5.19E+05
MR-508 arcjet	1800	2.25E-01	502	870	7.50	0.04	7.05E+05
650-s arcjet	2000	2.01E-01	650	900	7.50	0.04	6.51E+05
XIPS-13	500	1.78E-02	2585	6602	16.98	0.20	4.23E+05
NASA 30-cm ion	1822	7.30E-02	2814	8000	23.50	0.20	2.10E+06
SPT-100	1500	7.01E-02	1650	4000	16.30	0.20	1.01E+06
Lift propulsion systems							
H ₂ arcjet	10,000	6.0E-01	1200	1500	20	0.10	3.24E+06
Ion	2500	1.3E-01	3200	8000	30	0.15	3.74E+06
SPT/Hall	10,000	8.2E-01	1500	4000	25	0.15	1.18E+07

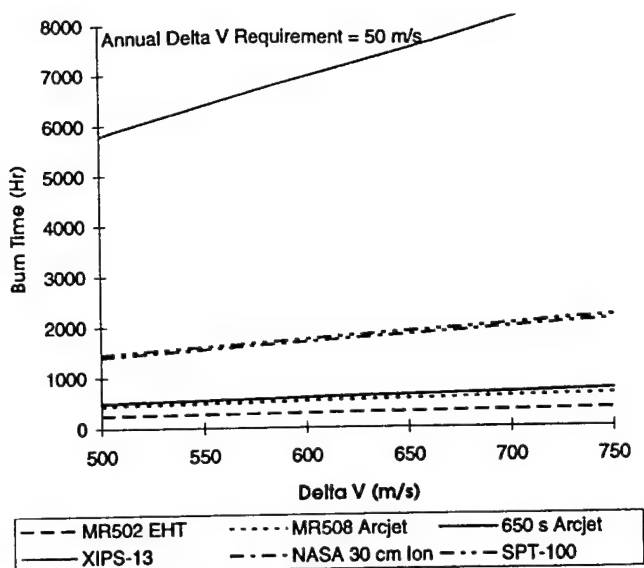


Fig. 2 Comparison of thruster burn time for hold maneuvers.

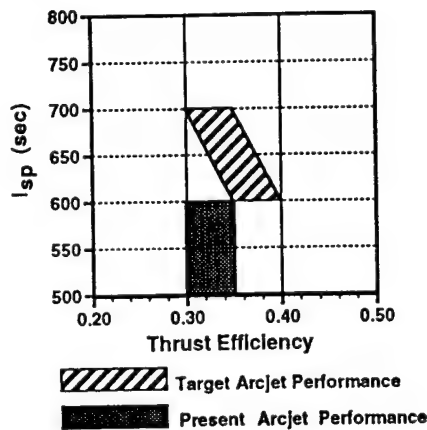


Fig. 3 Advanced arcjet performance for hold and move missions.

Move

On-orbit maneuvering of satellites is of increasing interest to users. This category encompasses orbit adjustment (e.g., circularization), plane changes, and E-W repositioning, among others. In the past, satellite assets have been launched and inserted into orbits that were more or less fixed for the life of the satellite. New demands for lower cost systems are driving users toward a different strategy, employing fewer satellites that are capable of moving as needs change. For rapid repositioning (i.e., 30 days or less), the ΔV required for one 180-deg repositioning maneuver is approximately the same as 1 year of N-S stationkeeping. The use of EP systems thus enables such missions.

A typical mission in this category is E-W repositioning of a GEO satellite. Figure 4 shows the results of a comparison of total propulsion system mass between candidate EP systems for an E-W maneuver halfway around the equator. To enable a direct comparison, a maneuver time of 21 days was selected. Power available for the EP systems was assumed to be limited to 2.0 kW because a typical military satellite has less onboard power than similar communications satellites. Actual power for each system was determined by their demonstrated capabilities as shown in Table 1.

The results show the effect of the lower inert mass of the arcjet system trading against the higher I_{sp} of the ion and Hall thrusters. The EHT and XIPS-13 thrusters are not competitive on a system mass basis for this mission and are not discussed. The SPT-100 Hall thruster system weighs less than the MR-

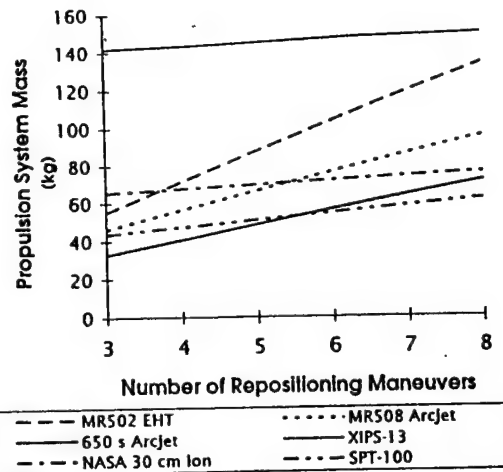


Fig. 4 Comparison of propulsion system mass for move missions.

508 arcjet over the entire range. The 30-cm ion engine trades poorly with the MR-508 arcjet below five repositioning maneuvers, but has a mass advantage if more than six maneuvers are desired. The advanced arcjet design (650 s) surpasses the ion engine and is competitive with the Hall thruster over the entire range. While not shown here, these trade studies have also revealed the importance of high arcjet thrust efficiency for time-critical maneuvers. Although this is of less consequence for the assumed mission duration, it is still of concern, especially if the desired maneuver time is much less than the assumed 21 days.

The approximate move mission performance ranges for an N_2H_4 arcjet are the same as the hold maneuver (Fig. 3). The main reason to select an arcjet for on-orbit maneuvering is once again increased I_{sp} . The thrust efficiency must be maintained for the arcjet to retain its burn-time advantage, particularly in situations where total maneuver durations of 10–14 days are desired.

Lift

The final mission category examined is orbit transfer or lift. Mission planners have long evaluated the concept of an electric orbit transfer vehicle (EOTV).^{8–10} EOTVs have the major advantage of large propellant mass savings relative to chemical upper stages. The major drawback to EOTV systems is the long trip times required to complete the transfers. Preventing the trip times from becoming excessively long requires that power levels for the EOTV increase to the 30–50-kW range. High-power levels such as these require large (200–300 m²) thin blanket deployable solar arrays, which currently can cost up to two million dollars per kilowatt. Minimizing the power requirement is therefore desirable to maintain a reasonable cost and size for the solar arrays.

A typical lift mission example is the deployment of a defense support program (DSP) satellite (2500 kg) to GEO from a LEO parking orbit. Figure 5 shows the results of a trade between EP thruster systems for this mission. The thruster performance parameters are listed under the Lift Propulsion Systems heading in Table 1. EOTV power level was assumed to be 30 kW for all concepts. The EP systems all save considerable propellant mass over the chemical system. Trip times shown in parentheses indicate an advantage for the arcjet because of its higher T/P . The hydrogen (H_2) arcjet must achieve an I_{sp} of 1300 s and a thrust efficiency of 40% to be mass competitive and maintain its trip time advantage. This represents the minimum acceptable performance and, as shown in Fig. 6, is not within the range of current performance capability. H_2 arcjet technology for EOTV missions is the area with the largest gap between current capability and required performance.

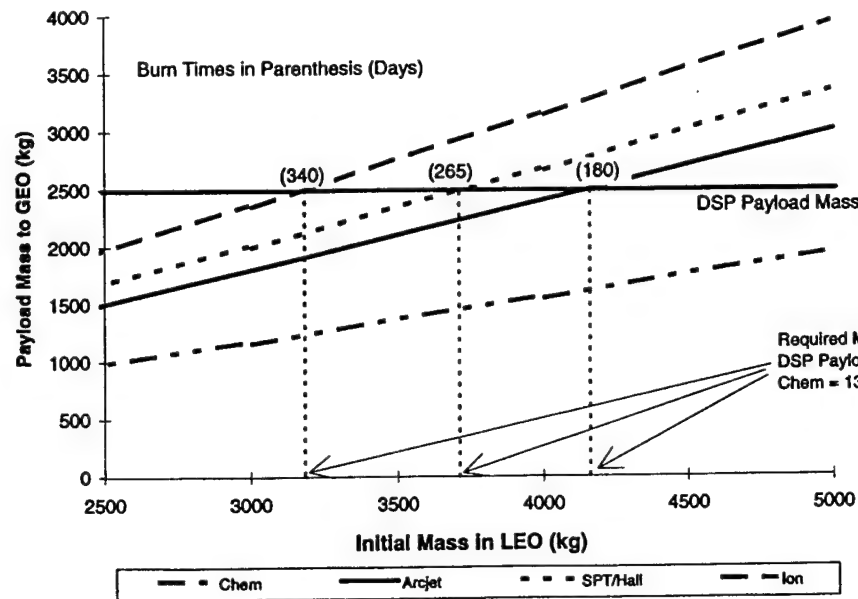


Fig. 5 Payload mass comparison for DSP-class satellite lift maneuver.

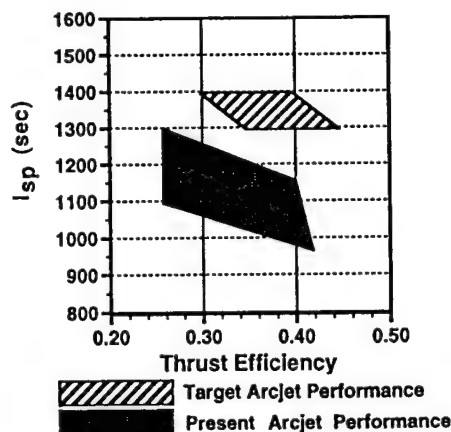


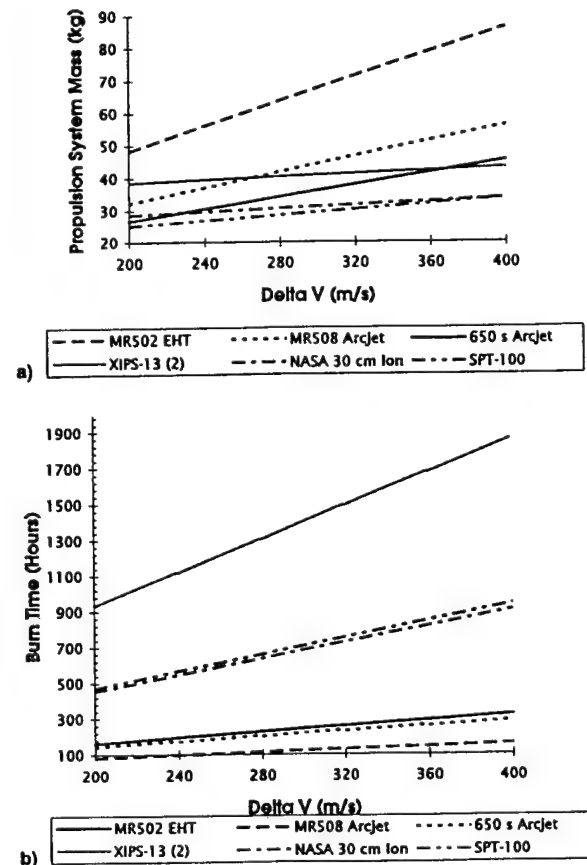
Fig. 6 Hydrogen arcjet performance target for lift missions.

Another example of a lift mission is orbit acquisition for a LEO constellation. Examples of such constellations are the Iridium network and the Teledesic system now in concept definition.¹¹ These constellations involve large numbers of satellites in many orbit planes. The initial insertion into a parking orbit is accomplished by putting 4–10 satellites on a single launch vehicle. From the parking orbit, each satellite must then be raised to its final altitude and moved to its operational position. Assumed performance parameters for the thruster systems are the same as for hold and move missions. System power was assumed to be 5.0 kW.

Figure 7a and 7b show the results of a comparison of EP devices for a representative LEO acquisition mission, such as the deployment of a 700-kg satellite to an orbital altitude between 500–1000 km. The results show that the arcjet I_{sp} must be improved to be mass competitive with the Hall thruster and ion engine. The arcjet T/P again provides a burn time advantage over all the other EP concepts. Figure 8 shows the development emphasis for this class of arcjet thruster is toward improved I_{sp} , while maintaining or slightly increasing η .

Arcjet Development Strategies

The improvements required to meet the next-generation performance goals can be realized only if new designs are able to achieve some measure of control over the key physical processes described earlier and shown in Fig. 1. Figure 9 illus-

Fig. 7 Summary of electric thruster system trades for LEO orbit acquisition: a) dependence of system mass and b) burn time on ΔV requirements.

trates a generic arcjet performance map that will serve as background for this discussion. Each curve represents the variation of η and I_{sp} with \dot{m} for one value of P_N . P_N/\dot{m} increases and \dot{m} decreases along each curve in the direction of increasing I_{sp} . Note that a maximum value for h is shown for each curve. Recent H_2 arcjet experiments have shown that I_{sp} is strongly influenced by frozen-flow losses below this maximum, and by thermal losses above it.¹² As P_N/\dot{m} increases, the time scale

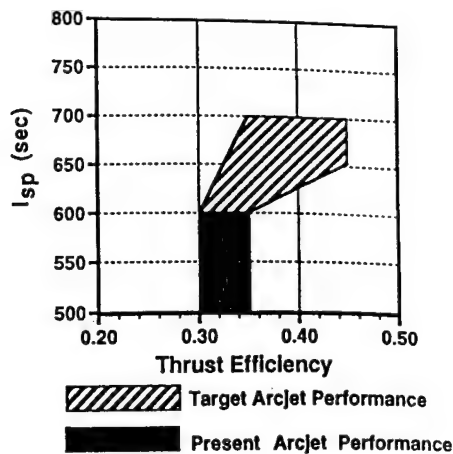


Fig. 8 Arcjet performance target for LEO orbit acquisition.

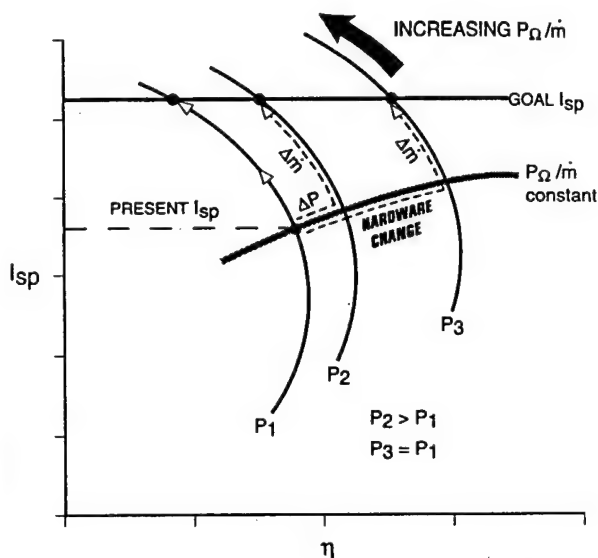


Fig. 9 Generic arcjet performance map showing three paths to achieve higher I_{sp} .

associated with diffusion and thermal conduction become significant compared to the plasma transit time. Operation at high P_0/\dot{m} —high I_{sp} is thus limited largely by thermal rather than frozen-flow losses. Above some critical value of P_0/\dot{m} , the energy flux to the anode severely degrades thruster efficiency and reduces thruster life. It follows that a critical value for P_0/\dot{m} can be defined, at least qualitatively, in terms of the maximum steady-state energy flux that the anode can tolerate.

Consider the I_{sp} value indicated by the solid line in Fig. 9 as an advanced hold or move mission goal and curve P_1 to be representative of present thruster performance at constant power. Three design options exist to provide higher I_{sp} and greater mission flexibility:

1) Maintain P_0 and decrease \dot{m} following curve P_1 to reach the I_{sp} goal. This is the short-term arcjet development strategy. Higher performance is being pursued by simply reducing \dot{m} at constant P_0 . The success of this approach depends upon the development of anode materials that are capable of withstanding significantly higher energy fluxes.

2) Increase P_0 to the P_2 value along a line of constant P_0/\dot{m} and then decrease \dot{m} to reach the I_{sp} goal. This option requires operating the arcjet at higher P_0 and higher \dot{m} . Note that increases in thruster power would still be accompanied by a reduction in \dot{m} to attain the design goal.

3) Maintain P_0 ($P_3 = P_1$), increase η via hardware improvements, and decrease \dot{m} to reach the I_{sp} goal. This is the most

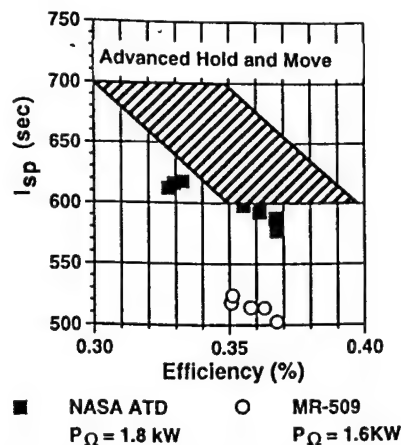


Fig. 10 State-of-the-art and advanced arcjet performance requirements for hold and move missions.

difficult of the three strategies since certain key physical processes must be controlled to produce higher η s.

Figure 10 illustrates the state-of-the-art performance levels of low-power N_2H_4 thrusters for hold and move missions. The graph shows the variation of I_{sp} with η for the NASA Advanced Technology Development thruster operating at 1.8 kW and the Olin Aerospace Model MR-509 thruster operating at 1.6 kW. The shaded box represents the advanced mission requirements outlined in the previous section. Extrapolation of these data to higher I_{sp} makes it clear that simply increasing P_0/\dot{m} (option 1) will not suffice. It is also unlikely that onboard power available for advanced low-power thrusters will significantly increase. This means that simply increasing the bus power (option 2) will not provide any appreciable benefit. Option 2 is still viable for H_2 EOTV missions since power level, lifetime, and configuration (e.g., the use of two 10-kW or four 5-kW thrusters) are somewhat flexible. Trip time constraints and the cost of solar arrays, however, will drive the EOTV configuration toward the highest achievable T/P . From these considerations, it is evident that improving thruster designs to increase operating efficiency (option 3) is the best strategy to achieve the next-generation performance and lifetime goals. This approach also affords the greatest technology leverage since high- η design concepts can be applied to a broad range of arcjet power classes without affecting their T/P advantage.

Management of Energy Transport Within the Anode

The choice of arcjet anode materials represents the true starting point for discussions of performance improvement. Any improvement in the efficiency of the basic plasma processes will directly add to benefits derived from new electrode materials or from novel schemes to process the electrode energy flux. Performance requirements force the anode material to operate at the highest P_0/\dot{m} it can tolerate over the thruster's useful life. The data of Fig. 11 show the variation of $(P_c/\dot{m})^{1/2}$ (a measure of the inverse of constrictor diameter) with time for life tests of a conventional low-power N_2H_4 arcjet operating at 1.8 kW and mission-averaged I_{sp} of 600 s. The symbols represent the behavior of the same anode geometry for three different materials: W-100, W-2%ThO₂, and W-4%Re-0.3%HfC. The solid line indicates an acceptable rate of increase for this parameter derived from the flight qualification data of MR-508, operating at 1.6 kW and approximately 500-s I_{sp} .

The underlying problem identified by these data is not that the anode fails, but rather that T/P falls off as the constrictor diameter decreases, and eventually, the thruster no longer satisfies the mission requirements. For example, increasing the power from 1.6 to 1.8 kW produces large increases in $(P_c/\dot{m})^{1/2}$ for both pure W-100 and W-2%ThO₂, and greatly reduces

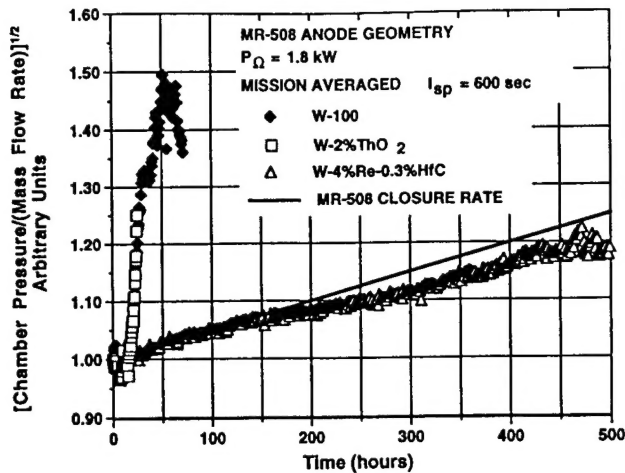


Fig. 11 Arcjet chamber pressure variation caused by anode thermal effects.

the probability of flight qualification. The constrictor closure rate of the W-4%Re-0.3%HfC anode, however, falls below and even improves upon that of present flight qualified designs. This demonstrates that improvements in electrode thermal properties can permit operation at higher I_{sp} or P_n/\dot{m} with considerable gains in performance and life.

In addition to the development of new anode materials, other ways to efficiently process higher thermal fluxes must also be developed. An obvious choice is to simply cool critical regions of the anode with the incoming propellant. For example, consider the benefit of providing regenerative passages in a 10-kW H_2 arcjet thruster. A gain of nearly five percentage points in η at 10 kW with P_n/\dot{m} ranging from 100 to 175 MJ/kg has been reported in recent work.¹³ The maximum measured efficiency was approximately 40% at $P_n/\dot{m} = 150$ MJ/kg. A thermal analysis using measured temperatures indicated that the regenerative efficiency achieved in this test series was approximately 94%.

It is our opinion that improvements in anode materials or energy processing capability will not by themselves permit operation at the performance levels desired for advanced applications. Also, a question remains whether regenerative concepts can be successfully applied to low-power geometries, primarily because of their small size and high inlet propellant temperatures.

Management of Plasma Energy and Mass Transport

Estimates for the distribution of electrical energy among the various plasma processes described in Fig. 1 are shown in Fig. 12. The charts are drawn for H_2 arcjets operating at a nominal P_n of 1.5 and 10 kW. The values for each category are taken from numerical performance estimates.^{13,14} Note that the thrust energy does not change significantly even when P_n increases by an order of magnitude. There is, however, a significant reapportionment of energy between the frozen-flow and thermal loss categories. This is largely because of the increase in \dot{m} of the higher power thruster and the corresponding decrease in flow transit time relative to molecular transport times. Similar trends are anticipated for other more complex propellants such as N_2H_4 . The loss categories with the greatest potential for improved performance are frozen-flow and thermal. Frozen-flow losses may be further split into energies associated with translation, rotation, vibration, electronic excitation (considered negligible), dissociation, and ionization. The thermal category includes radiative losses from the plasma and the anode as well as conduction to the anode and supporting structures. Finally, the thrust category is taken to be only the directed kinetic energy of the arcjet. If velocity profile losses are small, its value should be similar in magnitude to the conventional thrust efficiency.

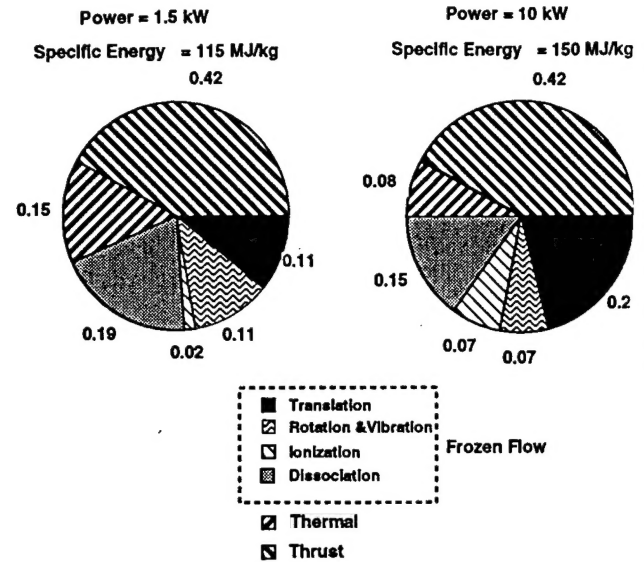


Fig. 12 Output energy distribution for low and intermediate power hydrogen arcjets.

Achieving control of the mass and energy transport between the plasma and the anode is a key element of this strategy. The difficulty that arises is that the physical processes contributing to the loss in performance are strongly coupled. For example, the plasma residence time can be increased in high density regions of the arcjet with a dramatic increase in ionization and atomic recombination rates (zone 3, Fig. 1). However, without special consideration given to the anode design, little of the additional chemical energy released will be converted to useful thrust. Instead, it will be transported by molecular diffusion to the anode surface and realized as thermal loss. Increased thermal loads resulting from this process reduce thruster lifetime.

The ability to manage the plasma-anode energy transfer requires an understanding of arcjet plasma physics, including the dynamics of the arc attachment. Unfortunately, the hostile physical environment and small size limit attempts to measure the state of the interior flow. The bulk of the diagnostics to date involve measurements of external flowfield parameters: chemical composition, and surface properties. Internal dynamics have been left to numerical models. The logic for this approach rapidly becomes circular since the confidence in such predictions rests on the fidelity of the measurements used to validate them. Much remains to be done to develop sound engineering design tools to transition from concept to practice.

Approach to Performance Model Development

The use of sophisticated numerical techniques to predict arcjet performance has grown considerably with the transition of the arcjet into flight application. Early work employing simplified plasma dynamics and equilibrium chemistry^{15,16} has been replaced by full Navier-Stokes solvers. These approaches typically include finite rate chemistry and transport properties, Maxwell's equations, and some model for energy transport across electrode boundaries. At the present time, single-fluid, single-temperature (1-F) models represent state-of-the-art design capability.^{17,18} Such models have shown reasonable agreement with experiment, particularly when the plasmadynamic solution is coupled with the anode thermal distribution. The self-consistent treatment of the anode and plasma is essential at high P_n/\dot{m} where material failure is anticipated. Any numerical evaluation of novel high-performance concepts without this capability must be held suspect.

Figures 13 and 14 show a comparison of a 1-F model predictions with measured values for velocity and temperature of excited state H atoms at the exit plane of a low-power H

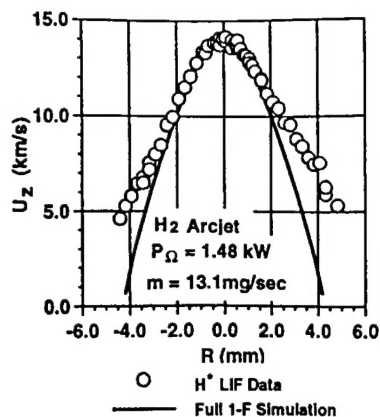


Fig. 13 Comparison of measured and predicted exit plane velocity profiles.

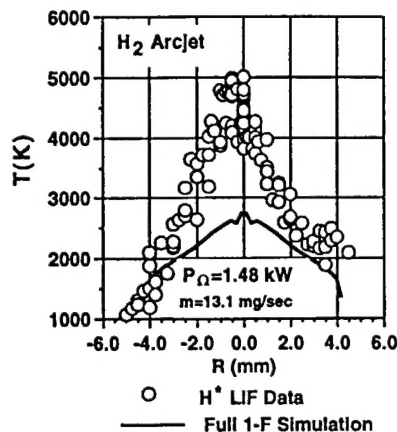


Fig. 14 Comparison of measured and predicted exit plane temperature profiles.

arcjet.¹⁹ The arcjet operating conditions were $P_0 = 1.5$ kW and $\dot{m} = 13.1$ mg/s. The agreement between predictions and measurements for both velocity and temperature is remarkably good. Similar agreement has been demonstrated for P_0/\dot{m} ranging from 50 to 125 MJ/kg (i.e., a factor of 2.5 in P_0). Although such results are encouraging, the fully coupled 1-F approach is not without its caveats. The validity of transport properties and chemical rate mechanisms at the plasma temperatures are only the most obvious of the uncertainties. Perhaps the most serious shortcoming of the 1-F models is that they do not accurately represent the electron transport or chemical activity in cooler regions of the plasma. This results in low estimates for electron population densities and σ_e and overestimates the ohmic dissipation near the anode. To compensate, some functional dependence of σ_e on P_0 and other plasma parameters must be assumed in the near-anode regions. The drawback of this approach is that the resulting performance predictions may only be valid for a limited range of electrode geometries and arcjet operating conditions.

In principle, a more general and physically correct representation of the plasmadynamics can be obtained using multifluid models.²⁰⁻²² In this approach, the different species are generally grouped into particle classes with similar temperatures (energies) and velocities.¹⁶ The dynamics of each particle class are then considered to evolve independently with the exchange of mass, momentum, and energy between classes expressed by appropriate models.

The choice of class structure depends on the nature of the problem and the detail to which the solution must be known. For example, 1-F models provide sufficiently accurate performance trends, but do not properly represent the cooler regions of the plasma. A two-fluid, two-temperature model with heavy

particle and electron classes will better represent the cooler regions, but cannot capture the physics of the electrode pre-sheath or primary sheath regions. Consideration of the ion and electron dynamics at the plasma-anode interface is required to reach this level of detail. To accurately estimate the full thermal loading of the anode, therefore, a multifluid performance model must include neutral, ion, and electron classes.

The more powerful multifluid approach provides a clearer view of the important physical processes and considerable modeling flexibility. However, it brings with it many of the difficulties of the 1-F models in addition to several others. The determination of appropriate transport properties and chemical rates remain important issues. In the multifluid case, however, species production and destruction must also be considered in terms of the exchange of mass, momentum, and energy between classes. Although the destination class of the product species is clear, the changes in class momentum and energy depend on the choice of reaction model.

The possibility of mass exchange between classes leads to one of the difficulties in applying this method, cases that involve a vanishing class population. Consider the situation at the root of the arc where the plasma is nearly fully ionized or along the anode wall near the exit plane where the ion and electron populations are considerably diminished. Under these conditions, the intraclass collision frequencies become so low that the classwise transport of mass and energy can no longer be based on continuum assumptions, for example, the Navier-Stokes equations. Note, however, that the minority class properties naturally limit to those of the majority class as a result of intraclass exchange processes. Multifluid solutions require approximations for the minority class dynamics that limit in a physically consistent way as their population becomes small. A minimum number density or floor can be imposed throughout the plasma, but a value must be chosen a priori that is small enough to represent the physics, yet large enough to avoid physically implausible results.¹⁸

Finally, the description of mass and energy transport at the electrode boundaries requires appropriate boundary conditions for each of the particle classes. The motion of charged particles remains coupled to neutrals to the extent that the plasma remains collisional. If the electrode surface is chemically active, the surface recombination rate of ions and electrons also sets a boundary condition on the production of neutral class species. The choice of surface chemistry model will therefore have a strong influence on estimates for current attachment and energy transport across the electrode surface.²³ In practice, such boundary conditions have proven to be stiff and difficult to implement. Although the use of the number density floor mentioned earlier may alleviate this problem, a perhaps better alternative would be to develop integral models of the near-electrode region.

Considering these modeling options, a development path that builds upon the strengths of both the single- and multifluid models may be advanced. The general objective would be to develop an understanding of internal arcjet dynamics sophisticated enough to develop and evaluate competing design options. Experimentally validated 1-F approaches would continue to provide guidance for experiments and the evaluation of new electrode configurations. Their application would provide timely and accurate performance predictions for propellants and operating conditions appropriate for advanced hold, lift, and move missions. This will require, at a minimum, a much improved description of the plasma physics in regions near the electrodes.

Multifluid modeling techniques should be developed to describe the arcjet plasmadynamics from a first principles point of view. These detailed multifluid models, along with complementary diagnostics, will serve as investigative tools to identify and to demonstrate an understanding of the critical performance issues. An obvious near-term goal of this effort would be to develop physical models that relate the far-field

plasma conditions, current density, and surface reactivity to the anode thermal loading. This work would contribute to the development of a generic wall model to improve single-fluid performance estimates.

Approach to Arcjet Diagnostic Development

The development of high-fidelity diagnostics to interrogate both the arcjet plasma and electrode surfaces is critical to the validation of numerical models as well as the measurement of advanced concept performance. The basic suite of measurements taken during an arcjet life test include current, voltage, propellant feed pressure, mass flow rate, temperature, and thrust. From these parameters one then derives I_{sp} and η and a qualitative measure of thruster health. It is clear that such data do not provide detailed information concerning energy and mass transport within the arcjet. Recent efforts have been made to employ advanced diagnostic techniques with experiment setups carefully designed to isolate the critical phenomena. Examples include the manufacture of anodes especially configured to measure current distributions,²⁴ internal plasma temperatures,²⁵ spectroscopic measurements of excited state species in the plume,²⁶⁻²⁹ and particle fluxes in the plume.²⁵

Preferred measurement techniques do not alter the flowfield or electrical characteristics of the plasma, are independent of electrode configuration, and can be used over a wide range of operating conditions. Such measurements should determine the distribution of energy among the different loss modes as a function of arcjet operating condition. This provides a means to evaluate global changes in performance that result from design changes. For example, the simultaneous measurement of frozen-flow and thermal losses at high P_0/\dot{m} is essential since, at least for conventional geometries, they trade in an almost one-to-one fashion. This is a formidable objective since it requires the measurement of species concentrations, temperatures or energies, and velocities as a function of operating condition.

A partial view of the frozen-flow and thermal loss dynamics can be constructed by combining recent results of emission spectroscopy, laser-induced fluorescence (LIF), and thermal imaging measurements. Emission spectroscopy has been used to identify major contributors to frozen-flow losses. For example, it can provide estimates of H^* number density at the exit plane of H_2 arcjets.¹² This data can then be related via nonequilibrium rate models to the local electron and ion number densities. For sufficiently high number densities, Stark broadening of the excited state emission can also provide a more direct estimate of the electron or ion number density. Having arrived at this estimate, some measure of the exit plane velocity distribution is needed to determine the local ion flux and therefore, the total ionization loss. The first experimental measurements of low-power H_2 arcjet exit plane velocities have been obtained for H atoms over a range of P_0/\dot{m} using LIF techniques.¹⁵ These velocity profiles can be used with the number density data to estimate ionization losses. Perhaps more importantly, the fact that 1-F arcjet performance model predictions correlate reasonably well with these measurements (see Fig. 13) allows the extension such loss estimates to conditions where LIF data are sparse or nonexistent.

As shown in Fig. 12, the energy tied up in ionization represents only a small fraction of the total frozen-flow loss in hydrogen arcjets. The fact that the ion population also increases as the total frozen-flow loss increases offers the hope that it can be taken as a trend indicator. For example, one could hypothesize that an electrode configuration that produces lower ionization losses also produces lower total frozen-flow losses. This requires the measurement and correlation of the major species number densities with model predictions. In particular, the primary objective should be the determination of the number densities of the neutral products of dissociation, since they represent the largest contributors to the dissociation losses. Efforts toward this objective have so far met with only limited success.³⁰

The measurement of the interior surface thermal loading and the resultant thermal losses presents another technical challenge. Some success has been achieved using full thermal models of the arcjet. This method typically assumes a certain thermal loss and iterates upon the spatial variation of energy flux on interior surfaces to achieve a match between the predicted and measured exterior surface temperatures. When an acceptable agreement has been obtained, one can estimate the total conductive, convective, and radiative energy exchange associated with the exterior and interior surfaces. The shortcomings of this approach are twofold. First, thermocouples cannot survive the arcjet's high steady-state anode surface temperatures. The lack of temperature data greatly increases the uncertainty of the loading estimates since radiation from the anode exterior is the largest contributor to the thermal loss category. Second, and most important, the exterior surface temperature profile is not uniquely determined by the interior surface fluxes, i.e., the exterior temperatures are insensitive to variations in the assumed internal loading profiles.

The first shortcoming has been addressed in most respects by thermal imaging of the anode exterior surfaces.^{11,12} These techniques provide a nearly continuous measure of the surface temperatures and greatly increase the sensitivity of the iterative scheme described earlier. If necessary, further refinements in the loading distribution may be obtained using profiles predicted by numerical performance models.

The second shortcoming can only be solved by direct measurement of the interior surface temperature or energy flux distribution. The development of diagnostic techniques to accomplish this task should receive a high priority. If arcjet designs are to move toward significantly higher P_0/\dot{m} , the processes that occur at the plasma-electrode boundary must be better understood and predicted with a reasonable degree of confidence. It follows then, that nonintrusive measurements must be made in the interior of the arcjet, or in arcjet-similar plasmas, to gain insight into the critical physics and validate models of the key processes.

Summary

Arcjet technology offers significant benefits over other electric propulsion options for many advanced mission applications. The impact of the arcjet on hold, move, and lift mission capabilities will be significant if next-generation arcjets can demonstrate sufficiently high I_{sp} . A number of design options were discussed, including operation at decreased mass flow, increased power, and increased efficiency. It appears that the only realistic way to achieve the desired I_{sp} is to improve upon present thrust efficiencies by reducing both frozen-flow and thermal losses. The objective is to reduce surface energy densities by controlling the transport of mass and energy to the anode surface. Improvements should include the continued refinement and validation of single-fluid models to provide timely performance estimates, the use of first principles multi-fluid models to investigate critical transport processes, the extension of these models to general performance estimates, and the development of diagnostic techniques to query the plasma and interior surfaces. In this endeavor, the approach to measurement and modeling development are intimately coupled.

Adopting this approach has the added benefit that the arcjet T/P and lifetime advantage over other electric propulsion devices remains unchallenged. Moreover, improvements in basic process efficiencies will build directly on efficiency gains from improvements in electrode material properties and advanced schemes to process high-energy fluxes. The design principles derived from this effort will apply to all classes of arcjets and all propellants.

Acknowledgment

The authors wish to thank David Q. King for his many helpful discussions and technical contributions to this effort.

References

- ¹Chan, A. K., Zondervan, K. P., and Smith, W. B., "Solar Electric Propulsion Assessment," Aerospace Corp., TOR-93(3501)-2, Los Angeles, CA, Dec. 1993.
- ²Smith, R. D., Yano, S. E., Armbruster, K., Roberts, C. R., Lichtin, D. A., and Beck, J. W., "Flight Qualification of a 1.8 kW Hydrazine Arcjet System," *Proceedings of the 23rd International Electric Propulsion Conference*, Electric Rocket Propulsion Society, Seattle, WA, 1993, pp. 93-107 (Paper 93-007).
- ³Lichon, P. G., and Sankovic, J., "Development and Demonstration of a 600-Second Mission-Average I_{sp} Arcjet," *Journal of Propulsion and Power*, Vol. 12, No. 6, 1996, pp. 1018-1025.
- ⁴Beattie, J. R., Williams, J. D., and Robson, R. R., "Flight Qualification of a 18-mN Xenon Ion Thruster," *Proceedings of the 23rd International Electric Propulsion Conference*, Electric Rocket Propulsion Society, Seattle, WA, 1993, pp. 971-978 (Paper 93-106).
- ⁵Garner, C. E., Polk, J. E., Pless, L. C., Goodfellow, K. D., and Brophy, J. R., "Performance Evaluation and Life Testing of the SPT-100," *Proceedings of the 23rd International Electric Propulsion Conference*, Electric Rocket Propulsion Society, Seattle, WA, 1993, pp. 823-839 (Paper 93-091).
- ⁶Ebert, W. L., Kowal, S. J., and Sloan, R. F., "Operational NOVA Spacecraft Teflon-Pulsed Plasma Thruster System," AIAA Paper 89-2497, July 1989.
- ⁷Pollard, J., Janson, S., and Cohan, R., "Electric Propulsion Flight Experience and Technology Readiness," Aerospace Corp., ATR-93(8344)-2, Los Angeles, CA, July 1993.
- ⁸Miller, T. M., and Seaworth, G. B., "Mission Factors Affecting Cost Optimization of Solar Electric Orbital Transfer Vehicles," *Proceedings of the 23rd International Electric Propulsion Conference*, Electric Rocket Propulsion Society, Seattle, WA, 1993, pp. 1825-1834 (Paper 93-202).
- ⁹Schmidt, W. M., "Analysis of Expendable EOTVs," AIAA Paper 90-2572, July 1990.
- ¹⁰Sponable, J. M., and Penn, J. P., "Electric Propulsion for Orbit Transfer: A Case Study," *Journal of Propulsion and Power*, Vol. 5, 1989, p. 445.
- ¹¹Hoskins, W. A., Kull, A. E., Nesser, W. M., and Butler, G. W., "Measurement of Energy Deposition Modes in an Intermediate Power Hydrogen Arcjet," *Proceedings of the 23rd International Electric Propulsion Conference*, Electric Rocket Propulsion Society, Seattle, WA, 1993, pp. 2008-2019 (Paper 93-216).
- ¹²Butler, G. W., Cassady, R. J., and Hoskins, W. A., "Performance of Advanced Concept Hydrogen Arcjet Anodes," *Proceedings of the 23rd International Electric Propulsion Conference*, Electric Rocket Propulsion Society, Seattle, WA, 1993, pp. 1949-1962 (Paper 93-211).
- ¹³Cappelli, M. A., and Storm, V., private communication, Stanford Univ., Stanford CA, June 1993.
- ¹⁴Stine, H. A., and Watson, V. R., "The Theoretical Enthalpy Distribution of Air in Steady Flow Along the Axis of a Direct-Current Electric Arc," NASA TN DD-1331, 1962.
- ¹⁵Watson, V. R., and Pegot, E. B., "Numerical Calculations for the Characteristics of a Gas Flowing Axially Through a Constricted Arc," NASA TN D-4042, June 1967.
- ¹⁶Rhodes, R., and Keefer, D., "Modeling Arcjet Space Thrusters," AIAA Paper 91-1994, June 1991.
- ¹⁷Butler, G. W., Kashiwa, B. A., and King, D. Q., "Numerical Modeling of Arcjet Performance," AIAA Paper 90-1474, June 1990.
- ¹⁸Cappelli, M. A., Liebeskind, J. G., Hanson, R. K., Butler, G. W., and King, D. Q., "A Comparison of Arcjet Plume Properties to Model Predictions," AIAA Paper 93-0820, Jan. 1993.
- ¹⁹Burgers, J. M., *Flow Equations for Composite Gases*, Academic, New York, 1969.
- ²⁰Butler, G. W., and King, D. Q., "Single and Two Fluid Simulations of Arcjet Performance," AIAA Paper 92-3104, July 1992.
- ²¹Miller, S., and Martinez-Sanchez, M., "Non-Equilibrium Numerical Simulation of Radiation-Cooled Arcjet Thrusters," *Proceedings of the 23rd International Electric Propulsion Conference*, Electric Rocket Propulsion Society, Seattle, WA, 1993, pp. 2032-2050 (Paper 92-218).
- ²²Meeks, E., "A Multi-Fluid Model of Near-Electrode Plasma Behavior," AIAA Paper 93-2103, June 1993.
- ²³Curran, F. M., and Manzella, D. H., "The Effect of Electrode Configuration on Arcjet Performance," AIAA Paper 89-2722, July 1989.
- ²⁴Zube, D. M., and Myers, R. M., "Nonequilibrium in a Low Power Arcjet Nozzle," *Journal of Propulsion and Power*, Vol. 9, No. 4, 1993, p. 545; also AIAA Paper 91-2113, July 1991.
- ²⁵Hoskins, W. A., Kull, A. E., and Butler, G. W., "Measurement of Population and Temperature Profiles in an Arcjet Plume," AIAA Paper 92-3240, June 1992.
- ²⁶Manzella, D. H., Curran, F. M., Zube, D. M., and Myers, R. M., "Preliminary Plume Characteristics of an Arcjet Thruster," AIAA Paper 90-2645, July 1990.
- ²⁷Janson, S. W., Welle, R. P., Schulthess, D. R., and Cohen, R. B., "Arcjet Plume Characterization Part II: Optical Diagnostic Results," AIAA Paper 90-2643, July 1990.
- ²⁸Zube, D. M., and Auwete-Kurtz, M., "Spectroscopic Arcjet Diagnostic Under Thermal Equilibrium and Nonequilibrium Conditions," AIAA Paper 93-1792, June 1993.
- ²⁹Pollard, J. E., "Arcjet Plume Studies Using Molecular Beam Mass Spectrometry," *Proceedings of the 23rd International Electric Propulsion Conference*, Electric Rocket Propulsion Society, Seattle, WA, 1993, pp. 1212-1227 (Paper 93-132).
- ³⁰Manzella, D. H., and Cappelli, M. A., "Vacuum Ultraviolet Absorption in a Hydrogen Arcjet," AIAA Paper 92-3564, July 1992.

A
c
c
c
E
e
f
j
k
k
n
n
n
P
C
K
K
7

u
Δ
δ
ρ
G
t